Feasibility analysis of using inverse modeling for estimating field-scale evapotranspiration in maize and soybean fields from soil water content monitoring networks

Foad Foolad[1], Trenton E. Franz[2], Tiejun Wang[2, 3], Justin Gibson[2], Ayse Kilic[1, 2], Richard G. Allen[4], Andrew Suyker[2]

[1]Civil Engineering Department, University of Nebraska-Lincoln, USA

[2]School of Natural Resources, University of Nebraska-Lincoln, USA

[3]Institute of Surface-Earth System Science, Tianjin University, P.R. China

[4]Kimberly Research and Extension Center, University of Idaho, USA

***Keywords*:** Evapotranspiration; Soil Water Content; Inverse Modeling; Soil Hydraulic Parameters; Cosmic-Ray Neutron Probe

Corresponding author T.E. Franz (tfranz2@unl.edu)

Abstract

In this study the feasibility of using inverse vadose zone modeling for estimating field scale actual evapotranspiration (ET_a) was explored at a long-term agricultural monitoring site in eastern Nebraska. Data from both point scale soil water content (*SWC*) sensors and the area-average technique of Cosmic-Ray Neutron Probes were evaluated against independent ET_a estimates from a co-located Eddy-Covariance tower. While this methodology has been successfully used for estimates of groundwater recharge, it was essential to assess the performance of other components of the water balance such as ET_a. In light of recent evaluations of Land Surface Models (LSM) independent estimates of hydrologic state variables and fluxes are critically needed benchmarks. The results here indicate reasonable estimates of daily and annual ET_a from the point sensors, but with highly varied soil hydraulic function parameterizations due to local soil texture variability. The results of multiple soil hydraulic parameterizations leading to equally good ET_a estimates is consistent with the hydrological principle of equifinality. While this study focused on one particular site, the framework can be easily applied to other *SWC* monitoring networks across the globe. The value added products of groundwater recharge and ET_a flux from the *SWC* monitoring networks will provide additional and more robust benchmarks for the validation of LSM that continues to improve their forecast skill. In addition, the value added products of groundwater recharge and ET_a often have more direct impacts on societal decision making than *SWC* alone. Water flux impacts human decision making from policies on the long-term management of groundwater resources (recharge), to yield forecasts (ET_a), and to optimal irrigation scheduling (ET_a). Illustrating the societal benefits of *SWC* monitoring is critical to insure the continued operation and expansion of these public datasets.

1. Introduction

Evapotranspiration (*ET*) is an important component in terrestrial water and surface energy balance. In the United States, *ET* comprises about 75% of annual precipitation, while in arid and semiarid regions *ET* comprises more than 90% of annual precipitation (Zhang et al., 2001; Glenn et al., 2007; Wang et al., 2009a). As such, an accurate estimation of *ET* is critical in order to predict changes in hydrological cycles and improve water resource management (Suyker et al., 2008; Anayah and Kaluarachchi, 2014). Given the importance of *ET*, an array of measurement techniques at different temporal and spatial scales have been developed (c.f., Maidment, 1992; Zhang et al., 2014), including lysimeter, Bowen ratio, Eddy-Covariance (EC), and satellite-based surface energy balance approaches. However, simple, low-cost, and accurate field-scale measurements of actual *ET* (ET_a) still remain a challenge due to the uncertainties of available estimation techniques (Wolf et al., 2008; Li et al., 2009; Senay et al., 2011; Stoy, 2012). For instance, field techniques, such as EC and Bowen ratio, can provide relatively accurate estimation of local ET_a, but are often cost prohibitive for wide-spread use beyond research applications (Baldocchi et al., 2001; Irmak, 2010). By comparison, satellite-based remote sensing techniques are far less costly for widespread spatial coverage (Allen et al., 2007), but are limited by their accuracy, temporal sampling frequency (e.g., Landsat 8 has a 16-day overpass), and technical issues that further limit temporal sampling periods (e.g., cloud coverage during overpass) (Chemin and Alexandridis, 2001; Xie et al., 2008; Li et al., 2009; Kjaersgaard et al., 2012).

As a complement to the above mentioned techniques, recent studies have used process-based vadose zone models (VZMs) for estimating field-scale ET_a with reasonable success, particularly in arid and semi-arid areas (Twarakavi et al., 2008; Izadifar and Elshorbagy, 2010; Galleguillos et al., 2011; Wang et al., 2016). Although VZMs are time and cost effective for estimating field-scale ET_a, they generally require complex model parameterizations and inputs, some of which are not readily available (e.g., soil hydraulic parameters and plant physiological parameters; c.f. Wang et al., 2016). In order to address the issue of missing soil hydraulic parameters, a common approach is to use pedotransfer functions to convert readily available soil information (e.g., texture, bulk density, etc.) to soil hydraulic parameters (Wösten et al., 2001); however, significant uncertainties are usually associated with this method for estimating local scale water fluxes (Wang et al., 2015). In fact, Nearing et al. (2016) identified soil hydraulic property estimation as the largest source of information lost when evaluating different land surface modeling schemes versus a soil moisture benchmark. Poor and uncertain parameterization of soil hydraulic properties is a clear weakness of land surface models (LSMs) predictive skill in sensible and latent heat fluxes (Best et al., 2015). This problem will continue to compound with the continuing spatial refinement of hyper-resolution LSM grid cells to less than 1 km (Wood et al., 2011).

In order to address the challenge of field scale estimation of soil hydraulic properties, here we utilize inverse modeling for estimating soil hydraulic parameters based on field measurements of soil water content (*SWC*) (c.f. Hopmans and Šimunek, 1999; Ritter et al., 2003). While VZM-based inverse approaches have already been examined for estimating groundwater recharge (e.g., Jiménez-Martínez et al., 2009; Andreasen et al., 2013; Min et al., 2015; Ries et al., 2015; Turkeltaub et al., 2015; Wang et al., 2016), its application for ET_a estimation has not been adequately tested. Moreover, we note that simultaneous estimation of *SWC* states and surface energy fluxes within LSMs is complicated by boundary conditions, model parameterization, and model structure (Nearing et al., 2016). With the incorporation of regional soil datasets in LSMs like Polaris (Chaney et al., 2016), effective strategies for estimating ground truth soil hydraulic properties from existing *SWC* monitoring networks (e.g., SCAN, CRN, COSMOS, State/National Mesonets, c.f. Xia et al. (2015)) will become critical for continuing to improve the predictive skill of LSMs.

The aim of this study is to examine the feasibility of using inverse VZM for estimating field scale ET_a based on long-term local meteorological and *SWC* observations for an Ameriflux (Baldocchi et al., 2001) EC site in eastern Nebraska, USA. We note that while this study focused on one particular study site in eastern Nebraska, the methodology can be easily adapted to a variety of *SWC* monitoring networks across the globe (Xia et al., 2015), thus providing an extensive set of benchmark data for use in LSMs. The remainder of the paper is organized as follows. In the methods section we will describe the widely used VZM, Hydrus-1D (Šimunek et al., 2013), used to obtain soil hydraulic parameters. We will assess the feasibility of using both profiles of in-situ *SWC* probes as well as the area-average *SWC* technique from Cosmic-Ray Neutron Probes (CRNP). In the results section we will compare simulated ET_a resulted from calibrated VZM with independent ET_a estimates provided by EC observations. Finally, a sensitivity analysis of key soil and plant parameters will be presented.

2. Materials and Methodology

2.1 Study Site

The study site is located in eastern Nebraska, USA at the University of Nebraska Agricultural and Development Center near Mead. The field site (US-Ne3, Figure 1a, 41.1797° N, 96.4397° W) is part of the Ameriflux Network (Baldocchi et al., 2001) and has been operating continually since 2001. The regional climate is of a continental semiarid type with a mean annual precipitation of 784 mm/year (according to the Ameriflux US-Ne3 website). According to the Web Soil Survey Data (Soil Survey Staff, 2016, http://websoilsurvey.nrcs.usda.gov/), the soils at the site are comprised mostly of silt loam and silty clay loam (Figure 1b and Table 1). Soybean and maize are rotationally grown at the site under rainfed conditions, with the growing season beginning in early May and ending in October (Kalfas et al., 2011). Since 2001, crop management practices (i.e., planting density, cultivars, irrigation, and herbicide and pesticide applications) have been applied in accordance with standard best management practices prescribed for production-scale maize systems (Suyker et al., 2008). More detailed information about site conditions can be found in Suyker et al. (2004) and Verma et al. (2005).

An EC tower was constructed at the center of the field (Figure 1 and Figure 2a), which continuously measures water, energy, and CO_2 fluxes (e.g., Baldocchi et al., 1988). At this field, sensors are mounted at 3.0 m above the ground when the canopy is shorter than 1.0 m. At canopy heights greater than 1.0 m, the sensors are then moved to a height of 6.2 m until harvest in order to have sufficient upwind fetch (in all directions) representative of the cropping system being studied (Suyker et al., 2004). In this study, hourly latent heat flux measurements were integrated to daily values and then used for calculating daily EC ET_a integrated over the field scale. Detailed information on the EC measurements and calculation procedures for ET_a are given in Suyker and Verma (2009). Hourly air temperature, relative humidity, horizontal wind speed, net radiation, and precipitation were also measured at the site. Destructive measurements of leaf area index (*LAI*) were made every 10 to 14 days during the growing season at the study site (Suyker et al., 2005). We note that the *LAI* data were linearly interpolated to provide daily estimates. Theta probes (TP) (Delta-T Devices, Cambridge, UK) were installed at 4 locations in the study field with measurement depths of 10, 25, 50, and 100 cm at each location to monitor hourly *SWC* in the root zone (Suyker et al., 2008). Here, we denote these four locations as TP 1 (41.1775° N, 96.4442° W), TP 2 (41.1775° N, 96.4428° W), TP 3 (41.1775° N, 96.4402° W), and TP 4 (41.1821° N, 96.4419° W) (Figure 1b). Daily precipitation (*P*) and reference evapotranspiration (ET_r) computed for the tall (alfalfa) reference crop using the ASCE standardized Penman-Monteith equation (ASCE-EWRI 2005) are shown in Figure 3 for the study period (2007–2012) at the study site.

In addition, a CRNP (model CRS 2000/B, HydroInnova LLC, Albuquerque, NM, USA, 41.1798 N°, 96.4412° W) was installed near the EC tower (Figure 1b and 2b) on 20 April 2011. The CRNP measures hourly moderated neutron counts (Zreda et al., 2008, 2012), which are converted into *SWC* following standard correction procedures and calibration methods (c.f., Zreda et al., 2012). In addition, the changes in above-ground biomass were removed from the CRNP estimates of *SWC* following Franz et al. (2015). The CRNP measurement depth (Franz et al., 2012) at the site varies between 15-40 cm, depending on *SWC*. Note for simplicity in this analysis we assume the CRNP has an effective depth of 20 cm (mean depth of 10 cm) for all observational periods. The areal footprint of the CRNP is ~250+/-50 m radius circle (see Desilets and Zreda 2013 and Köhli et al., 2015 for details). Here we assume for simplicity the EC and CRNP footprints are both representative of the areal-average field conditions.

2.2. Model setup

2.2.1 Vadose Zone Model

The Hydrus-1D model (Šimunek et al., 2013), which is based on the Richards equation, was used to calculate ET_a. The setup of the Hydrus-1D model is explained in detail by Jiménez-Martínez et al. (2009), Min et al. (2015), and Wang et al. (2016), and only a brief description of the model setup is provided here. Given the measurement depths of the Theta Probes, the simulated soil profile length was chosen to be 175 cm with 176 nodes at 1 cm intervals. An atmospheric boundary condition with surface runoff was selected as the upper boundary. This allowed the occurrence of surface runoff when precipitation rates were higher than soil infiltration capacity or if the soil became saturated. According to a nearby USGS monitoring well (Saunders County, NE, USGS 411005096281502, ~2.7 km away), the depth to water tables was greater than 12 m during the study period. Therefore, free drainage was used as the lower boundary condition.

Based on ASCE Penman-Monteith equation, ET_r values can be computed for either grass or alfalfa and then using crop-specific coefficients daily potential evapotranspiration (ET_p) can be calculated. Here daily ET_r values were calculated for the tall (0.5 m) ASCE reference (ASCE-EWRI, 2005), and daily potential evapotranspiration (ET_p) was calculated according to FAO 56 (Allen et al., 1998):

$$ET_p(t) = K_C(t) \times ET_r(t) \qquad (1)$$

where Kc is a crop-specific coefficient at time t. The estimates of growth stage lengths and Kc values for maize and soybean suggested by Allen et al. (1998) and Min et al. (2015) were adopted in this study. In order to partition daily ET_p into potential transpiration (T_p) and potential evaporation (E_p) as model inputs, Beer's law (Šimunek et al., 2013) was used as follows:

$$E_p(t) = ET_p(t) \times e^{-k \times LAI(t)} \qquad (2)$$

$$T_p(t) = ET_p(t) - E_p(t) \qquad (3)$$

where k [-] is an extinction coefficient with a value set to 0.5 (Wang et al., 2009b) and LAI [L^2/L^2] is leaf area index described in the previous section. The root water uptake, $S(h)$, was simulated according to the model of Feddes et al. (1978):

$$S(h) = \alpha(h)\times S_p \quad (4)$$

where $\alpha(h)$ [-] is the root-water uptake water stress response function and varies between 0 and 1 depending on soil matric potentials, and S_p is the potential water uptake rate and assumed to be equal to T_p. The summation of actual soil evaporation and actual transpiration is ET_a.

Since the study site has annual cultivation rotations between soybean and maize, the root growth model from the Hybrid-Maize Model (Yang et al., 2004) was used to model the root growth during the growing season:

$$\begin{cases} if\ D < MRD,\ D = \frac{AGDD}{GDD_{Silking}} MRD \\ \quad or\ D = MRD \end{cases} \quad (5)$$

where D (cm) is plant root depth for each growing season day, MRD is the maximum root depth (assumed equal to 150 cm for maize and 120 cm for soybean in this study following Yang et al., 2004), $AGDD$ is the accumulated growing degree days, and $GDD_{Silking}$ is the accumulated GDD at the silking point (e.g., accumulated plant GDD approximately 60-70 days after crop emergence). GDD for each growing season day was calculated as:

$$GDD = \frac{T_{max} - T_{min}}{2} - T_{base} \quad (6)$$

where T_{max} and T_{min} are the maximum and minimum daily temperature (°C), respectively, and T_{base} is the base temperature set to be 10° C following McMaster and Wilhelm (1997) and Yang et al.

(1997). Finally, the Hoffman and van Genuchten (1983) model was used to calculate root distribution. Further details about the model can be found in Šimunek et al. (2013).

2.2.2 Inverse modeling to estimate soil hydraulic parameters

Inverse modeling was used to estimate soil hydraulic parameters for the van Genuchten-Mualem model (Mualem, 1976; van Genuchten, 1980):

$$\theta(h) = \begin{cases} \theta_r + \frac{\theta_s - \theta_r}{(1+|\alpha h|^n)^m}, h < 0 \\ \theta_s,\ h \geq 0 \end{cases} \quad (7)$$

$$K(S_e) = K_s \times S_e^{\,l} \times [1-(1-S_e^{\,1/m})^m]^2 \quad (8)$$

where θ [L^3/L^3] is volumetric *SWC*; θ_r [L^3/L^3] and θ_s [L^3/L^3] are residual and saturated water content, respectively; h [L] is pressure head; K [L/T] and K_s [L/T] are unsaturated and saturated hydraulic conductivity, respectively; and S_e (=$(\theta-\theta_r)/(\theta_s-\theta_r)$) [-] is saturation degree. With respect to the fitting factors, α [1/L] is inversely related to air entry pressure, n [-] measures the pore size distribution of a soil with m=1–1/n, and l [-] is a parameter accounting for pore space tortuosity and connectivity.

Daily *SWC* data from the four TP locations and CRNP location were used for the inverse modeling. Based on the measurement depths of the TPs, the simulated soil columns were divided into four layers for TP locations (i.e., 0-15 cm, 15-35 cm, 35-75 cm, and 75-175 cm), which led to a total of 24 hydraulic parameters (θ_r, θ_s, α, n, K_s, and l) to be optimized based on observed *SWC* values. In order to efficiently optimize the parameters, we used the method outlined in Turkeltaub et al. (2015). Since Hydrus-1D is limited to optimizing a maximum of 15 parameters at once and that the *SWC* of the lower layers changes more slowly and over a smaller range than the upper layers, the van Genuchten parameters of the upper two layers were first optimized, while the parameters of the lower two layers were fixed. Then, the optimized van Genuchten parameters of the upper two layers were kept constant, while the parameters of the lower two layers were optimized. The process was continued until there were no further improvements in the optimized hydraulic parameters or until the changes in the lowest sum of squares were less than 0.1%. Given the sensitivity of the optimization results to the initial guesses of soil hydraulic parameters in the Hydrus model, soil hydraulic parameters from six soil textures were used as initial inputs for the optimizations at each location (Carsel and Parish, 1988), including sandy clay loam, silty clay loam, loam, silt loam, silt, and clay loam. Based on the length of available *SWC* data from the TP measurements, the periods of 2007, 2008-2010, and 2011-2012 were used as the spin-up, calibration, and validation periods, respectively. Moreover, to minimize the impacts of freezing conditions on the quality of *SWC* measurements, data from January to March of each calendar year were removed (based on available soil temperature data) from the optimizations.

In addition to the TP profile observations, we used the CRNP area-average *SWC* in the inverse procedure to develop an independent set of soil parameters. The CRNP was assumed to provide *SWC* data with an average effective measurement depth of 20 cm at this study site. The observation point was therefore set at 10 cm. As a first guess and in the absence of other information, soil properties were assumed to be homogeneous throughout the simulated soil column with a length of 175 cm. Because the CRNP was installed in 2011 at the study site, the periods of 2011, 2012-2013, and 2014 were used as spin-up, calibration, and validation periods, respectively, for the optimization procedure.

The lower and upper bounds of each van Genuchten parameter are provided in Table 2. With respect to the goodness-of-fit assessment, Root Mean Square Error (RMSE) between simulated and observed *SWC* was chosen as the objective function to minimize in order to estimate the soil hydraulic parameters. The built in optimization procedure in Hydrus-1D was used to perform parameter estimation. A sensitivity analysis of the six soil model parameters was performed. In addition, three additional performance criteria, including Coefficient of Determination (R^2), Mean Average Error (MAE), and the Nash-Sutcliffe Efficiency (NSE) were used to further evaluate and validate the selected model behavior:

$$RMSE = \sqrt{\frac{1}{n}\sum_{i=1}^{n}(P_i - O_i)^2} \quad (9)$$

$$R^2 = \left(\frac{n(\sum_{i=1}^{n} P_i O_i) - (\sum_{i=1}^{n} P_i)(\sum_{i=1}^{n} O_i)}{\sqrt{[n\sum_{i=1}^{n} {P_i}^2 - (\sum_{i=1}^{n} P_i)^2][n\sum_{i=1}^{n} {O_i}^2 - (\sum_{i=1}^{n} O_i)^2]}}\right)^2 \quad (10)$$

$$MAE = \frac{1}{n}\sum_{i=1}^{n}|P_i - O_i| \quad (11)$$

$$NSE = 1 - \frac{\sum_{i=1}^{n}(P_i - O_i)^2}{\sum_{i=1}^{n}(O_i - \bar{O}_i)^2} \quad (12)$$

where n is the total number of *SWC* data points, O_i, and P_i, are respectively the observed and simulated daily *SWC* on day i, and $\bar{O}_i$ is the observed mean value. Based on the best scores (i.e., lowest RMSE values), the best optimized set of soil hydraulic parameters at each location were selected. Using the selected parameters, the Hydrus model was then run in a forward mode in order to estimate ET_a between 2007 and 2012. Finally, we note that the years 2004-2006 were used as a model spin-up period for the forward model and evaluation of ET_a because of the longer climate record length.

3. Results and Discussions

3.1 Vadose Zone Inverse Modeling Results

The time series of the average *SWC* from the four TP locations along with one standard deviation at each depth are plotted in Figure 4. Based on the large spatial standard deviation values (Figure 4), despite the relatively small spatial scale (~65 ha) and uniform cropping at the study site, *SWC* varies considerably across the site, particularly during the growing season. The comparison between *SWC* data from the CRNP and spatial average of *SWC* data at the four TP locations in the study field (i.e. average of 10 and 25 cm depths at TP locations) is presented in Figure 5. The daily RMSE between the spatial average of the TPs and CRNP data is 0.037 cm^3/cm^3, which is consistent with other studies that reported similar values in semiarid shrublands (Franz et al., 2012), German Forests (Bogena et al., 2013, Baatz et al., 2014), montane forests in Utah (Lv et al., 2014), sites across Australia (Hawdon et al., 2014), and a mixed land use agricultural site in Austria (Franz et al. 2016). We note that we would expect lower RMSE (~<0.02 cm^3/cm^3) with additional point sensors located at shallower depths and in more locations distributed across the study site. Nevertheless, the consistent behavior between the spatial mean *SWC* of TPs and the CRNP allows us to explore spatial variability of soil hydraulic properties within footprint using inverse modeling. This will be described in the next sections. The study period (2007-2012, Figure 6) contained significant inter-annual variability in precipitation. During the spin-up period in 2007, the annual precipitation (942 mm) was higher than the mean annual precipitation (784 mm), 2008 was a wet year (997 mm), 2009-2011 were near average years (715 mm), and 2012 was a record dry year (427 mm) with widespread drought across the region. Therefore, both wet and dry years were considered in the inverse modeling simulation period.

As an illustration, Figure 7 shows the daily observed and simulated *SWC* during the calibration (2008–2010) and validation (2011–2012) periods at the TP 1 location (the simulation results of the other three sites can be found in the supplemental Figures S1, S2, and S3). The results of objective function criterion (RMSE) and the other three performance criteria (e.g., R^2, MAE, and NSE) between simulated and observed *SWC* values at TPs locations are presented in Table 3.

In this research we define RMSE values less than 0.03 cm^3/cm^3 between observed and simulated *SWC* values as well-matched and RMSE between 0.03 and 0.06 cm^3/cm^3 as fairly well-matched. We note the target error range of satellite *SWC* products (e.g. SMOS and SMAP) is less than 0.04 cm^3/cm^3 (Entekhabi et al., 2010). Similar to previous studies (e.g., Jiménez-Martínez et al., 2009; Andreasen et al., 2013; Min et al., 2015; Wang et al., 2016), the results of all the performance criteria at TP locations show the capability of inverse modeling in estimation of soil hydraulic parameters. The results of the calibration period (2008-2010) indicate that the simulated and observed *SWC* values are in good agreement (i.e. well matched as defined above) throughout the entire period at most locations and depths (Figure 7 and Table 3). In addition, the simulated and observed *SWC* data are fairly well-matched at most locations and depths during the validation period (2011-2012), with notable differences during the second half of 2012 during the extreme drought conditions (Figure 7 and Table 3). Reasons for this disagreement in the observed and simulated *SWC* data will be discussed in the following sections.

The results of inverse modeling using the CRNP data also indicate the feasibility of using these data to estimate effective soil hydraulic parameters (Figure 8 and Table 4). Based on the performance criteria (Table 4), the simulated data are fairly well-matched with the observed *SWC* data during both the calibration and validation periods. Additional information from deeper soil probes or more complex modeling approaches such as data assimilation techniques (Rosolem et al., 2014, Renzullo et al., 2014) may be needed to fully utilize the CRNP data for the entire growing season. However, this was beyond the scope of the current study and merits further investigation given the global network of CRNP (Zreda et al., 2012) dating back to ~2011.

Table 5 summarizes the optimized van Genuchten parameters for the four different depths of the four TP locations and the single layer for the CRNP location. The optimized parameters were then used to estimate ET_a for the entire study period as an independent comparison to the EC ET_a data. The results of the ET_a evaluation will be discussed in the next section. According to the simulation results (Table 5), in most of the soil layers, the TP 4 location results in lower n, K_s, and higher θ_r values than the other 3 locations (TPs 1-3), suggesting either underlying soil texture variability in the field or texture dependent sensor sensitivity/calibration. As a validation for the simulation results, the publicly available Web Soil Survey Data (http://websoilsurvey.nrcs.usda.gov/) was used to explore whether the optimized van Genuchten parameters from the inverse modeling (Figure 1b and Table 2) agreed qualitatively with the survey data. Based on the Web Soil Survey Data, the soil at the TP 4 location contains higher clay percentage than the other locations. Meanwhile, the optimized parameters reflect the spatial pattern of soil texture in the field as shown by the Web Soil Survey Data (e.g., lower n and K_s values and higher θ_r values at the TP 4 location with finer soil texture). Physically, finer-textured soils generally have lower K_s and higher θ_r values (Carsel and Parrish, 1988). Moreover, the shape factor n is indicative of pore size distributions of soils. In general, finer soils with smaller pore sizes tend to have lower n values (Carsel and Parrish, 1988). The observed SWC at the TP 4 location is consistently higher than the average SWC of the other three locations (Figure S4 in supplemental materials), which can be partly attributed to the higher θ_r values at the TP 4 location

(Wang and Franz, 2015). Overall, the obtained van Genuchten parameters from the inverse modeling are in qualitatively good agreement with the available spatial distribution of soil texture in the study field, indicating the capability of using inverse VZM to infer soil hydraulic properties. Further work on validating the Web Soil Survey Data soil hydraulic property estimates is of general interest to the LSM community.

3.2 Comparison of modeled ET_a with observed ET_a

Because a longer set of climatic data was available at the study site (as compared to *SWC* data), we used 2004-2006 as a spin-up period. Using the best fit soil hydraulic parameters for the four TP locations and the single CRNP location, the Hydrus-1D model was then run in a forward mode to calculate ET_a over the entire study period (2007-2012). The simulated daily ET_a was then compared with the independent EC ET_a measurements using RMSE (Eq. (9)) as the evaluation criterion. In order to upscale TP ET_a estimation to the field/EC scale, we used the soil textural boundaries and areas defined by the Web Soil Survey Data map to compute a weighted average ET_a. In this research we consider RMSE values less than 1 mm/day between observed and simulated ET_a values as well-matched and RMSE values between 1 and 1.2 as fairly well-matched (Figure 9 and Table 6). The performance criterion results indicate that the simulated daily ET_a is in a better agreement with EC ET_a measurements at the TP 1-3 locations than at the TP 4 and CRNP locations (Table 6). However, based on the performance criteria from inverse modeling results and on the Web Soil Survey Data, we conclude that spatial heterogeneity of soil texture in the study field results in significant spatial variation in ET_a rates across the field (e.g., less ET_a occurs at the TP 4 location than from the other parts of the field). Here smaller ET_a rates at the TP 4 location are likely due to finer soil texture at this location, which makes it more difficult for the plant/roots to overcome potentials to extract water from the soil, thus leading to a lower ET_a rate and greater plant stress. In addition, higher surface runoff can be expected at the TP 4 location due to finer-textured soils (as we observed during our field campaigns). According to the simulation results the average surface runoff at the TP 4 location was about 44.8 mm/year from 2007 to 2012, while the average surface runoff at the other three locations (TPs 1-3) was around 10.6 mm/year, which partially accounts for the lower ET_a rates. We note that future work using historic yield maps may also be used to further elucidate the soil hydraulic property differences given the direct correlation between transpiration and yield.

Given that CRNPs have a limited observational depth and that only one single soil layer was optimized in the inverse model for the CRNP, one could expect the simulated daily ET_a from the CRNP to have larger uncertainty. Here we found an RMSE of 1.14 mm/day using the CRNP versus 0.91 mm/day for the upscaled TP locations. However, when the optimized soil parameters obtained from the CRNP data were used to estimate ET_a, the model did simulate daily ET_a fairly well during both non-growing and growing seasons in comparison to the EC ET_a measurements.

On the annual scale, ET_a measured by the EC tower accounted for 87% of annual P recorded at the site during the study period (Figure 6). Overall, the simulated annual ET_a at all the TP and CRNP locations is comparable to the annual ET_a measured by the EC tower, except during 2012 (Table 7), in which a severe drought occurred in the region. One explanation is that the plants extract more water from deeper layers under extreme drought conditions than what we defined as a maximum rooting depth (150 cm for maize and 120 cm for soybean) for the model, thus limiting the VZM ability to estimate ET_a accurately during the drought year (2012). In fact, based on the EC ET_a measurements at the study site, there was just 8.18% reduction in annual ET_a in 2012 than the average of the other years (2007-2011), while there were 29.58% and 35.75% reduction in annual simulated ET_a values respectively in upscaled TP and CRNP. This shows that although 2012 was a very dry year, the plants probably found most of the needed water by extracting water from deeper soil reservoirs. As previously mentioned we defined a maximum rooting depth for the model that could greatly impact the results. To further illustrate this point, a sensitivity analysis was performed on the maximum rooting depth and presented in the following section. However, we note that given the fact that EC ET_a estimation can have up to 20% uncertainty (Massman and Lee, 2002, and Hollineger and Richardson, 2005), and accounting for the natural spatial variability of ET_a due to soil texture and root depth growth uncertainties, the various ET_a estimation techniques performed fairly well. In fact, it is difficult to identify which ET_a estimation method is the most accurate method. These results are consistent with the concept of equifinality in hydrologic modeling given the complexity of natural systems (Beven and Freer, 2001). Moreover, the findings here are consistent with Nearing et al. (2016) that show information lost in model parameters greatly affects the soil moisture comparisons against a benchmark. However, soil parameterization was less important in the loss of information for the comparisons of *ET*/latent energy against a benchmark. Fully resolving these issues remains a key challenge to the land surface modeling community and the model's ability to make accurate predictions (Best 2015). The following section provides a detailed sensitivity analysis of the soil hydraulic parameters and root depth growth functions in order to begin to understand the sources of error in estimating ET_a from *SWC* monitoring networks.

3.3 Sensitivity analysis of soil hydraulic parameters and rooting depth

In this research we compared simulated ET_a with the measured EC ET_a. As expected some discrepancies between simulated and measured ET_a values existed. In order to begin to understand the key sources of error we performed a set of sensitivity analysis experiments on the estimated soil hydraulic parameters. Building on Wang et al. (2009b), a sensitivity analysis for a single homogeneous soil layer (6 parameters) and a 4-layer soil profile (24 parameters) was performed over the study period (2007–2012). Here we performed a preliminary sensitivity analysis by changing a single soil hydraulic parameter one at a time while keeping the other parameters constant (i.e. at the average value). Figure 10 illustrates the sensitivity results on simulated ET_a, indicating the soil hydraulic parameters have a range of sensitivities with tortuosity (*l*) being the least. We found that n and α were the most sensitive, particularly in the shallowest soil layer. This sensitivity to the shallowest soil layer provides an opportunity to use the CRNP observations, particularly in the early growing season (i.e. when evaporation dominates latent energy flux), to help constrain estimates of n and α. As the crop continues to develop (and transpiration contributes a relatively larger component of latent energy) additional information about deeper soil layers should be used to estimate soil hydraulic parameters or perform data assimilation. Moreover, the CRNP may be useful in helping constrain and parameterize soil hydraulic functions in simpler evaporation models widely used in remote sensing (c.f. Allen et al. 2007) and crop modeling (c.f. Allen et al. 1998).

Following the sensitivity analysis, we repeated the optimization experiment using only α, n, K_s, and used model default estimates for the other parameters in each layer. We found that the RMSE values were significantly higher (1.511 vs. 0.911 mm/day) than when considering all 24 parameters. We suspect that given the high correlation between soil hydraulic parameters (Carsel and Parrish 1988), that fixing certain parameters leads to a degradation in overall performance. We suggest further sensitivity analyses, in particular changing multiple parameters simultaneously or using multiple objective functions, be used to fully understand model behavior (c.f. Bastidas et al. 1999 and Rosolem et al. 2012).

A sensitivity analysis of ET_a by varying rooting depth is summarized in Figure 11. As would be expected with increasing rooting depth, higher ET_a occurred. In addition, Figure 11 illustrates a decreasing RMSE against EC observations for up to 200% increases. Again it is unclear if the EC observations are biased high or in fact rooting depths are much greater than typically considered in these models. The high observed EC values in the drought year of 2012 indicate that roots likely uptake water from below the 1 m observations. Certainly the results shown here further indicate the importance of root water uptake parameters in VZMs and LSMs, even in homogeneous annual cropping systems. While beyond the scope of this paper we refer the reader to the growing literature on the importance of root water uptake parameters on hydrologic fluxes (c.f. Schymanski et al. 2008 and Guswa 2012).

3.4 Applications and limitations of the vadose zone modeling framework

Given its simplicity and widespread availability of ground data, ET_r and Kc values are often used in a wide variety of applications to estimate ET_p and thus approximate ET_a. It is well known that SWC is a limiting factor affecting the assumption that $ET_p \sim ET_a$. On the other hand, we know that SWC observations are local in nature and not necessarily representative of ET_a footprint estimates. The key questions are: what is the value of SWC observations, how many profiles do we need to install in a footprint, and at which depths to constrain estimates of fluxes? The well instrumented and long-term study presented here allows us to start to answer these key questions. First we find that ET_p has an average annual value of 1064.9 mm as compared to EC at 612.5 mm (Table 7). By including individual SWC profiles (TP 1 to 4) and the CRNP in the VZM framework we are able to constrain our estimate of ET_a to between 525.3 and 643.1 mm and reduce ET_a RMSE from 1.992 mm/day to around 1 mm/day (Table 6). In addition, a range of soil hydraulic parameters for each depth and spatially averaged top layer can be estimated to help better constrain recharge fluxes simultaneously. Given the principle of equifinality in hydrologic systems, the VZM framework may lead to equally reasonable estimates of parameters which is a limitation of the method and LSMs in general. Based on our sensitivity analysis (Figure 10) the key parameters of α, n may greatly affect ET_a.

Although sparsely distributed, widespread state, national, and global meteorological observations paired with *SWC* profiles (Xia et al. 2015) and the VZM framework provide an opportunity to better constrain ET_a and local soil hydraulic functions. Moreover, where multiple *SWC* profile information is available a range of ET_a and soil hydraulic parameters can be estimated and thus considered in LSM data assimilation frameworks. The combination of basic metrological observations with a CRNP in the VZM framework further allows for estimates of upscaled soil hydraulic parameters with similar estimates of ET_a as found with individual *SWC* profiles. Moving forward, combining CRNP with deeper *SWC* observations from point sensors seems to be a reasonable strategy in order to average the inherent *SWC* variability in the near surface yet provide SWC constraints at depth, particularly as annual crops develop over the growing season.

4. Conclusions

In this study the feasibility of using inverse vadose zone modeling for field scale ET_a estimation was explored at an agricultural site in eastern Nebraska. Both point *SWC* sensors (TP) and area-average techniques (CRNP) were explored. This methodology has been successfully used for estimates of groundwater recharge but it was critical to assess the performance of other components of the water balance such as ET_a. The results indicate reasonable estimates of daily and annual ET_a but with varied soil hydraulic function parameterizations. The varied soil hydraulic parameters were expected given the heterogeneity of soil texture at the site and consistent with the principle of equifinality in hydrologic systems. We note that while this study focused on one particular site, the framework can be easily applied to other networks of *SWC* monitoring across the globe (Xia et al., 2015). The value added products of groundwater recharge and ET_a flux from the *SWC* monitoring networks will provide additional and more robust benchmarks for the validation of LSM that continue to improve their forecast skill.

5. Data availability

The climatic and EC data used in this research can be found at http://ameriflux.lbl.gov/. The TP *SWC* and *LAI* data in the study site are provided by Dr. Andrew Suyker and CRNP *SWC* are provided by Dr. Trenton E. Franz and both sets of data can be requested directly from the authors. The US soil taxonomy information is provided by Soil Survey Staff and is available online at http://websoilsurvey.nrcs.usda.gov/ (accessed in July, 2016). The remaining datasets are provided in the supplemental material associated with this paper.

Acknowledgments

This research is supported financially by the Daugherty Water for Food Global Institute at the University of Nebraska, NSF EPSCoR FIRST Award, the Cold Regions Research Engineering Laboratory through the Great Plains CESU, and an USGS104b grant. We sincerely appreciate the support and the use of facilities and equipment provided by the Center for Advanced Land Management Information Technologies, School of Natural Resources and data from Carbon Sequestration Program, the University of Nebraska-Lincoln. TEF would like to thank Eric Wood for his inspiring research and teaching career. No doubt the skills TEF learned while at Princeton in formal course work, seminars, and discussions with Eric will serve him well in his own career.

References

Allen, R. G., Pereira, L. S., Raes, D., & Smith, M. (1998). Crop evapotranspiration-guidelines for computing crop water requirements-FAO irrigation and drainage paper 56. FAO, Rome, 300(9), D05109.

Allen, R. G., Tasumi, M., & Trezza, R. (2007). Satellite-based energy balance for mapping evapotranspiration with internalized calibration (METRIC)—Model. Journal of Irrigation and Drainage Engineering, 133(4), 380-394.

Anayah, F. M., & Kaluarachchi, J. J. (2014). Improving the complementary methods to estimate evapotranspiration under diverse climatic and physical conditions. Hydrology and Earth System Sciences, 18(6), 2049-2064.

Andreasen, M., Andreasen, L. A., Jensen, K. H., Sonnenborg, T. O., & Bircher, S. (2013). Estimation of regional groundwater recharge using data from a distributed soil moisture network. Vadose Zone Journal, 12(3)

ASCE – EWRI. (2005). The ASCE Standardized reference evapotranspiration equation. ASCE-EWRI Standardization of Reference Evapotranspiration Task Comm. Report, ASCE Bookstore, ISBN 078440805, Stock Number 40805, 216 pages.

Baatz, R., Bogena, H., Franssen, H. H., Huisman, J., Qu, W., Montzka, C., et al. (2014). Calibration of a catchment scale cosmic-ray probe network: A comparison of three parameterization methods. Journal of Hydrology, 516, 231-244.

Baldocchi, D. D., Hincks, B. B., & Meyers, T. P. (1988). Measuring biosphere-atmosphere exchanges of biologically related gases with micrometeorological methods. Ecology, 1331-1340.

Baldocchi, D., Falge, E., Gu, L., & Olson, R. (2001). FLUXNET: A new tool to study the temporal and spatial variability of ecosystem-scale carbon dioxide, water vapor, and energy flux densities. Bulletin of the American Meteorological Society, 82(11), 2415.

Bastidas, L. A., H. V. Gupta, S. Sorooshian, W. J. Shuttleworth, and Z. L. Yang (1999), Sensitivity analysis of a land surface scheme using multicriteria methods, J. Geophys. Res.-Atmos., 104(D16), 19481-19490. doi:10.1029/1999jd900155.

Best, M., Abramowitz, G., Johnson, H., Pitman, A., Balsamo, G., Boone, A., et al. (2015). The plumbing of land surface models: Benchmarking model performance. Journal of Hydrometeorology, 16(3), 1425-1442.

Beven, K., & Freer, J. (2001). Equifinality, data assimilation, and uncertainty estimation in mechanistic modelling of complex environmental systems using the GLUE methodology. Journal of Hydrology, 249(1), 11-29.

Bogena, H., Huisman, J., Baatz, R., Hendricks Franssen, H., & Vereecken, H. (2013). Accuracy of the cosmic-ray soil water content probe in humid forest ecosystems: The worst case scenario. Water Resources Research, 49(9), 5778-5791.

Carsel, R. F., & Parrish, R. S. (1988). Developing joint probability distributions of soil water retention characteristics. Water Resources Research, 24(5), 755-769.

Chaney, N. W., Wood, E. F., McBratney, A. B., Hempel, J. W., Nauman, T. W., Brungard, C. W., et al. (2016). POLARIS: A 30-meter probabilistic soil series map of the contiguous United States. Geoderma, 274, 54-67.

Chemin, Y., & Alexandridis, T. (2001). Improving spatial resolution of ET seasonal for irrigated rice in Zhanghe, china. Paper Presented at the 22nd Asian Conference on Remote Sensing, 5. pp. 9.

Desilets, D., & Zreda, M. (2013). Footprint diameter for a cosmic-ray soil moisture probe: Theory and monte carlo simulations. Water Resources Research, 49(6), 3566-3575.

Entekhabi, D., E. G. Njoku, P. E. O'Neill, K. H. Kellogg, W. T. Crow, W. N. Edelstein, J. K. Entin, S. D. Goodman, T. J. Jackson, J. Johnson, J. Kimball, J. R. Piepmeier, R. D. Koster, N. Martin, K. C. McDonald, M. Moghaddam, S. Moran, R. Reichle, J. C. Shi, M. W. Spencer, S.

W. Thurman, L. Tsang, and J. Van Zyl (2010), The Soil Moisture Active Passive (SMAP) Mission, Proc. IEEE, 98(5), 704-716. doi:10.1109/jproc.2010.2043918.

Feddes, R. A., Kowalik, P. J., & Zaradny, H. (1978). Simulation of field water use and crop yield. Centre for Agricultural Publishing and Documentation.

Franz, T. E., Wahbi, A., Vreugdenhil, M., Weltin, G., Heng, L., Oismueller, M., et al. (2016). Using cosmic-ray neutron probes to monitor landscape scale soil water content in mixed land use agricultural systems. Applied and Environmental Soil Science, 2016.

Franz, T. E., Wang, T., Avery, W., Finkenbiner, C., & Brocca, L. (2015). Combined analysis of soil moisture measurements from roving and fixed cosmic ray neutron probes for multiscale real-time monitoring. Geophysical Research Letters, 42(9), 3389-3396.

Franz, T. E., Zreda, M., Ferre, T., Rosolem, R., Zweck, C., Stillman, S., et al. (2012). Measurement depth of the cosmic ray soil moisture probe affected by hydrogen from various sources. Water Resources Research, 48(8).

Galleguillos, M., Jacob, F., Prévot, L., Lagacherie, P., & Liang, S. (2011). Mapping daily evapotranspiration over a Mediterranean vineyard watershed. Geoscience and Remote Sensing Letters, IEEE, 8(1), 168-172.

Glenn, E. P., Huete, A. R., Nagler, P. L., Hirschboeck, K. K., & Brown, P. (2007). Integrating remote sensing and ground methods to estimate evapotranspiration. Critical Reviews in Plant Sciences, 26(3), 139-168.

Guswa, A. J. (2012), Canopy vs. Roots: Production and Destruction of Variability in Soil Moisture and Hydrologic Fluxes, Vadose Zone Journal, 11(3). doi:10.2136/vzj2011.0159.

Hawdon, A., McJannet, D., & Wallace, J. (2014). Calibration and correction procedures for cosmic-ray neutron soil moisture probes located across Australia. Water Resources Research, 50(6), 5029-5043.

Hollinger, D. Y., & Richardson, A. D. (2005). Uncertainty in eddy covariance measurements and its application to physiological models. Tree Physiology, 25(7), 873-885.

Hopmans, J.W., Šimunek, J., 1999. Review of inverse estimation of soil hydraulic properties. In: van Genuchten, M.Th. Leij, F.J., Wu, L. (Eds.), Proceedings of the International Workshop Characterization and Measurement of Hydraulic Properties of Unsaturated Porous Media. University of California, Riverside, 643–659.Irmak, S. (2010). Nebraska water and energy flux measurement, modeling, and research network (NEBFLUX). Transactions of the ASABE, 53(4), 1097-1115. Irmak, S. (2010). Nebraska water and energy flux measurement, modeling, and research network (NEBFLUX). Transactions of the ASABE, 53(4), 1097-1115.

Izadifar, Z., & Elshorbagy, A. (2010). Prediction of hourly actual evapotranspiration using neural networks, genetic programming, and statistical models. Hydrological Processes, 24(23), 3413-3425.

Jiménez-Martínez, J., Skaggs, T., Van Genuchten, M. T., & Candela, L. (2009). A root zone modelling approach to estimating groundwater recharge from irrigated areas. Journal of Hydrology, 367(1), 138-149.

Kalfas, J. L., Xiao, X., Vanegas, D. X., Verma, S. B., & Suyker, A. E. (2011). Modeling gross primary production of irrigated and rain-fed maize using MODIS imagery and CO 2 flux tower data. Agricultural and Forest Meteorology, 151(12), 1514-1528.

Kjaersgaard, J., Allen, R., Trezza, R., Robinson, C., Oliveira, A., Dhungel, R., et al. (2012). Filling satellite image cloud gaps to create complete images of evapotranspiration. IAHS-AISH Publication, 102-105.

Köhli, M., Schrön, M., Zreda, M., Schmidt, U., Dietrich, P., & Zacharias, S. (2015). Footprint characteristics revised for field-scale soil moisture monitoring with cosmic-ray neutrons. Water Resources Research, 51(7), 5772-5790.

Li, Z., Tang, R., Wan, Z., Bi, Y., Zhou, C., Tang, B., et al. (2009). A review of current methodologies for regional evapotranspiration estimation from remotely sensed data. Sensors, 9(5), 3801-3853.

Lv, L., Franz, T. E., Robinson, D. A., & Jones, S. B. (2014). Measured and modeled soil moisture compared with cosmic-ray neutron probe estimates in a mixed forest. Vadose Zone Journal, 13(12)

Maidment, D. R. (1992). Handbook of hydrology. McGraw-Hill Inc.

Massman, W., & Lee, X. (2002). Eddy covariance flux corrections and uncertainties in long-term studies of carbon and energy exchanges. Agricultural and Forest Meteorology, 113(1), 121-144.

McMaster, G. S., & Wilhelm, W. (1997). Growing degree-days: One equation, two interpretations. Agricultural and Forest Meteorology, 87(4), 291-300.

Min, L., Shen, Y., & Pei, H. (2015). Estimating groundwater recharge using deep vadose zone data under typical irrigated cropland in the piedmont region of the north china plain. Journal of Hydrology, 527, 305-315.

Mualem, Y. (1976). A new model for predicting the hydraulic conductivity of unsaturated porous media. Water Resources Research, 12(3), 513-522.

Nearing, G. S., Mocko, D. M., Peters-Lidard, C. D., Kumar, S. V., & Xia, Y. (2016). Benchmarking NLDAS-2 soil moisture and evapotranspiration to separate uncertainty contributions. Journal of Hydrometeorology, 17(3), 745-759.

Renzullo, L. J., Van Dijk, A., Perraud, J., Collins, D., Henderson, B., Jin, H., et al. (2014). Continental satellite soil moisture data assimilation improves root-zone moisture analysis for water resources assessment. Journal of Hydrology, 519, 2747-2762.

Ries, F., Lange, J., Schmidt, S., Puhlmann, H., & Sauter, M. (2015). Recharge estimation and soil moisture dynamics in a Mediterranean, semi-arid karst region. Hydrology and Earth System Sciences, 19(3), 1439-1456.

Ritter, A., Hupet, F., Muñoz-Carpena, R., Lambot, S., & Vanclooster, M. (2003). Using inverse methods for estimating soil hydraulic properties from field data as an alternative to direct methods. Agricultural Water Management, 59(2), 77-96.

Rosolem, R., H. V. Gupta, W. J. Shuttleworth, X. B. Zeng, and L. G. G. de Goncalves (2012), A fully multiple-criteria implementation of the Sobol' method for parameter sensitivity analysis, J. Geophys. Res.-Atmos., 117. doi:10.1029/2011jd016355.

Schaap, M. G., Leij, F. J., & Van Genuchten, M. T. (2001). Rosetta: A computer program for estimating soil hydraulic parameters with hierarchical pedotransfer functions. Journal of Hydrology, 251(3), 163-176.

Schymanski, S. J., M. Sivapalan, M. L. Roderick, J. Beringer, and L. B. Hutley (2008), An optimality-based model of the coupled soil moisture and root dynamics, Hydrology and Earth System Sciences, 12(3), 913-932.

Senay, G. B., Budde, M. E., & Verdin, J. P. (2011). Enhancing the simplified surface energy balance (SSEB) approach for estimating landscape ET: Validation with the METRIC model. Agricultural Water Management, 98(4), 606-618.

Šimunek, J., Šejna, M., Saito, H., Sakai, M., van Genuchten, M.T. (2013). The HYDRUS-1D Software Package for Simulating the One-Dimensional Movement of Water,Heat, and Multiple Solutes in Variably-Saturated Media, Version 4.17.Department of Environmental Sciences, University of California Riverside, Riverside, California, USA, 307 pp.

Soil Survey Staff, Natural Resources Conservation Service, United States Department of Agriculture. Web Soil Survey. Available online at http://websoilsurvey.nrcs.usda.gov/. Accessed in July, 2016.

Stoy, P. (2012). Evapotranspiration and energy flux observations from a global tower network with a critical analysis of uncertainties. AGU Fall Meeting Abstracts, 1. pp. 06.

Suyker, A., Verma, S., Burba, G., Arkebauer, T., Walters, D., & Hubbard, K. (2004). Growing season carbon dioxide exchange in irrigated and rainfed maize. Agricultural and Forest Meteorology, 124(1), 1-13.

Suyker, A. E., & Verma, S. B. (2008). Interannual water vapor and energy exchange in an irrigated maize-based agroecosystem. Agricultural and Forest Meteorology, 148(3), 417-427.

Suyker, A. E., & Verma, S. B. (2009). Evapotranspiration of irrigated and rainfed maize–soybean cropping systems. Agricultural and Forest Meteorology, 149(3), 443-452.

Suyker, A. E., Verma, S. B., Burba, G. G., & Arkebauer, T. J. (2005). Gross primary production and ecosystem respiration of irrigated maize and irrigated soybean during a growing season. Agricultural and Forest Meteorology, 131(3), 180-190.

Suyker, A. E., Verma, S. B., Burba, G. G., & Arkebauer, T. J. (2005). Gross primary production and ecosystem respiration of irrigated maize and irrigated soybean during a growing season. Agricultural and Forest Meteorology, 131(3), 180-190.

Turkeltaub, T., Kurtzman, D., Bel, G., & Dahan, O. (2015). Examination of groundwater recharge with a calibrated/validated flow model of the deep vadose zone. Journal of Hydrology, 522, 618-627.

Twarakavi, N. K. C., Šimůnek, J., & Seo, S. (2008). Evaluating interactions between groundwater and vadose zone using the HYDRUS-based flow package for MODFLOW. Vadose Zone Journal, 7(2), 757-768.

van Genuchten, M. T. (1980). A closed-form equation for predicting the hydraulic conductivity of unsaturated soils. Soil Science Society of America Journal, 44(5), 892-898.

Verma, S. B., Dobermann, A., Cassman, K. G., Walters, D. T., Knops, J. M., Arkebauer, T. J., et al. (2005). Annual carbon dioxide exchange in irrigated and rainfed maize-based agroecosystems. Agricultural and Forest Meteorology, 131(1), 77-96.

Wang, T., & Franz, T. E. (2015). Field observations of regional controls of soil hydraulic properties on soil moisture spatial variability in different climate zones. Vadose Zone Journal, 14(8)

Wang, T., Franz, T. E., Yue, W., Szilagyi, J., Zlotnik, V. A., You, J., et al. (2016). Feasibility analysis of using inverse modeling for estimating natural groundwater recharge from a large-scale soil moisture monitoring network. Journal of Hydrology, 533, 250-265.

Wang, T., Franz, T. E., & Zlotnik, V. A. (2015). Controls of soil hydraulic characteristics on modeling groundwater recharge under different climatic conditions. Journal of Hydrology, 521, 470-481.

Wang, T., Istanbulluoglu, E., Lenters, J., & Scott, D. (2009a). On the role of groundwater and soil texture in the regional water balance: An investigation of the Nebraska sand hills, USA. Water Resources Research, 45(10)

Wang, T., Zlotnik, V. A., Šimunek, J., & Schaap, M. G. (2009b). Using pedotransfer functions in vadose zone models for estimating groundwater recharge in semiarid regions. Water Resources Research, 45(4)

Wolf, A., Saliendra, N., Akshalov, K., Johnson, D. A., & Laca, E. (2008). Effects of different eddy covariance correction schemes on energy balance closure and comparisons with the modified bowen ratio system. Agricultural and Forest Meteorology, 148(6), 942-952.

Wood, E. F., Roundy, J. K., Troy, T. J., Van Beek, L., Bierkens, M. F., Blyth, E., et al. (2011). Hyperresolution global land surface modeling: Meeting a grand challenge for monitoring earth's terrestrial water. Water Resources Research, 47(5)

Wösten, J., Pachepsky, Y. A., & Rawls, W. (2001). Pedotransfer functions: Bridging the gap between available basic soil data and missing soil hydraulic characteristics. Journal of Hydrology, 251(3), 123-150.

Xia, Y., Ek, M. B., Wu, Y., Ford, T., & Quiring, S. M. (2015). Comparison of NLDAS-2 simulated and NASMD observed daily soil moisture. part I: Comparison and analysis. Journal of Hydrometeorology, 16(5), 1962-1980.

Xie, Y., Sha, Z., & Yu, M. (2008). Remote sensing imagery in vegetation mapping: A review. Journal of Plant Ecology, 1(1), 9-23.

Yang, H., Dobermann, A., Cassman, K. G., & Walters, D. T. (2004). Hybrid-maize. A Simulation Model for Corn Growth and Yield. Nebraska Cooperative Extension CD, 9.

Yang, W., Yang, L., & Merchant, J. (1997). An assessment of AVHRR/NDVI-ecoclimatological relations in Nebraska, USA. International Journal of Remote Sensing, 18(10), 2161-2180.

Zhang, L., Dawes, W., & Walker, G. (2001). Response of mean annual evapotranspiration to vegetation changes at catchment scale. Water Resources Research, 37(3), 701-708.

Zhang, Z., Tian, F., Hu, H., & Yang, P. (2014). A comparison of methods for determining field evapotranspiration: Photosynthesis system, sap flow, and eddy covariance. Hydrology and Earth System Sciences, 18(3), 1053-1072.

Zreda, M., Shuttleworth, W., Zeng, X., Zweck, C., Desilets, D., Franz, T., et al. (2012). COSMOS: The cosmic-ray soil moisture observing system. Hydrology and Earth System Sciences, 16(11), 4079-4099.

Zreda, M., Desilets, D., Ferré, T., & Scott, R. L. (2008). Measuring soil moisture content non-invasively at intermediate spatial scale using cosmic-ray neutrons. Geophysical Research Letters, 35(21).

List of Figures

Figure 1. Study site (Mead Rainfed/US-Ne3) location in Nebraska (a) and locations of Eddy-Covariance Tower (EC), Cosmic-Ray Neutron Probe (CRNP), Theta Probes (TPs), and variability of soil texture based on Web Soil Survey data at the study site, 2014 (b). See table 1 for soil descriptions.

Figure 2. Eddy-Covariance Tower (a) and Cosmic-Ray Neutron Probe (b) Located at the Mead Rainfed (US-Ne3) Site.

Figure 3. Daily precipitation (*P*) and reference evapotranspiration (ET_r) during the calibration (2008–2010) and validation (2011–2012) periods at the Mead Rainfed (US-Ne3) Site.

Figure 4. Temporal evolution of daily *SWC* (θ) at different soil depths. The black lines represent daily mean *SWC* (θ) calculated from TPs in 4 different locations at study site and the blue areas indicate one standard deviation.

Figure 5. Time series of daily CRNP and spatial average TP *SWC* (θ) data.

Figure 6. Annual precipitation (*P*) and annual actual evapotranspiration (ET_a) at the Mead Rainfed (US-Ne3) Site.

Figure 7. Daily observed and simulated *SWC* (θ) during the calibration (2008–2010) and validation (2011–2012) periods at TP 1 location. See supplemental figures for other comparisons.

Figure 8. Daily observed and simulated *SWC* (θ) during the calibration (2012–2013) and validation (2014) periods at the location of Cosmic-Ray Neutron probe.

Figure 9. Simulated daily *ETa* versus Observed daily *ETa* in different locations at the study site (2007-2012).

Figure 10. Sensitivity Analysis of Effect of Soil Hydraulic Parameters on average annual *ETa* values (2007-2012) for a single homogeneous soil layer (6 parameters) and for a 4-layer soil profile (24 parameters).

Figure 11. Sensitivity Analysis of Effect of Root Depth on *ETa* estimation for a single homogeneous soil layer profile. Note that root depth is in terms of percent depth as it is

dynamic over the growing period.

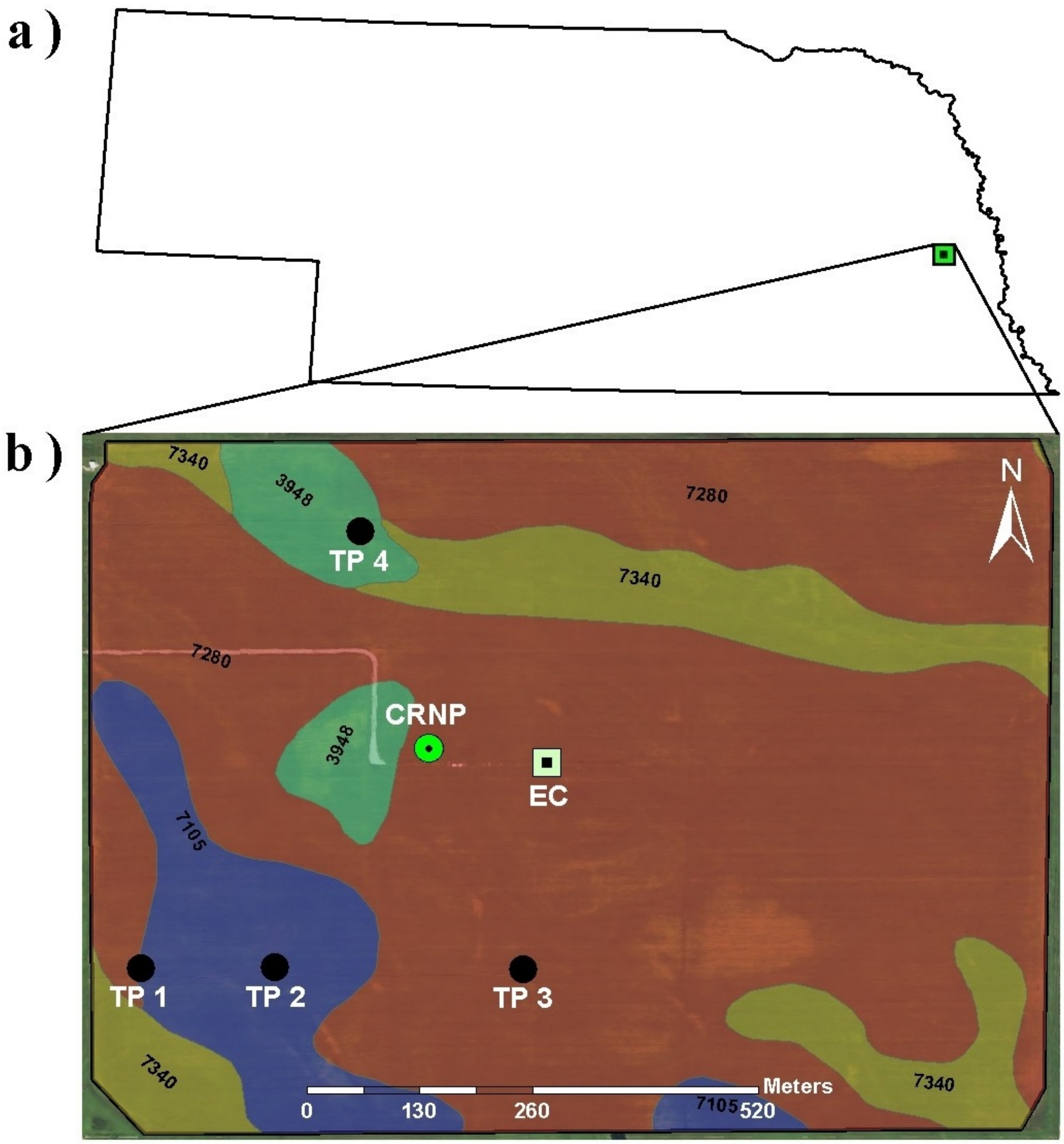

Figure 1. Study site (Mead Rainfed/US-Ne3) location in Nebraska (a) and locations of Eddy-Covariance Tower (EC), Cosmic-Ray Neutron Probe (CRNP), Theta Probes (TPs), and variability of soil texture based on Web Soil Survey data at the study site, 2014 (b). See table 1 for soil descriptions.

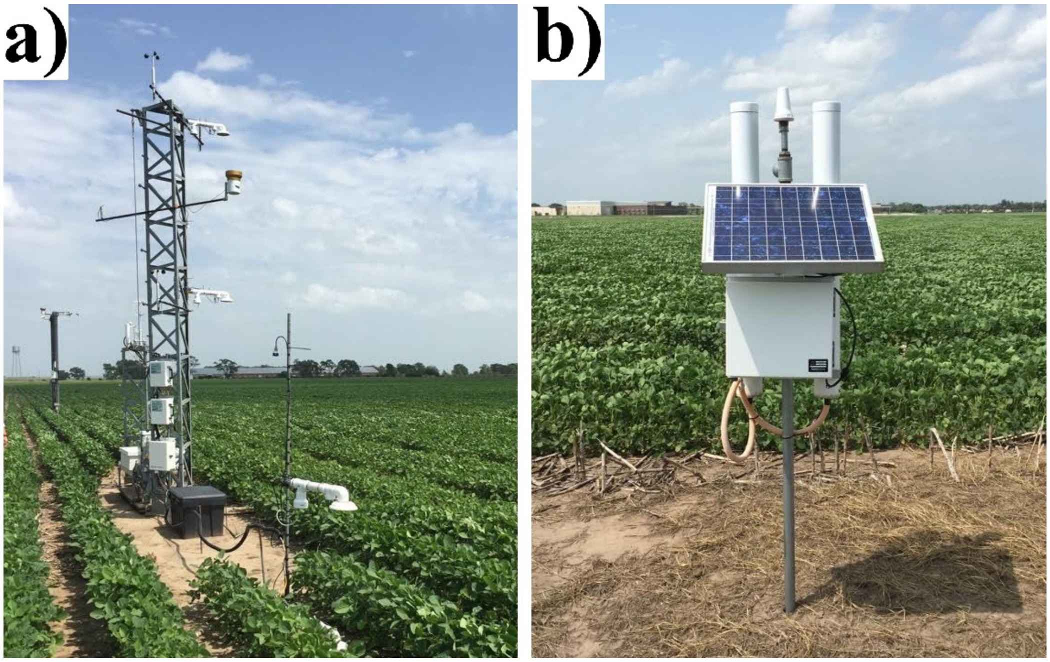

Figure 2. Eddy-Covariance Tower (a) and Cosmic-Ray Neutron Probe (b) Located at the Mead Rainfed (US-Ne3) Site.

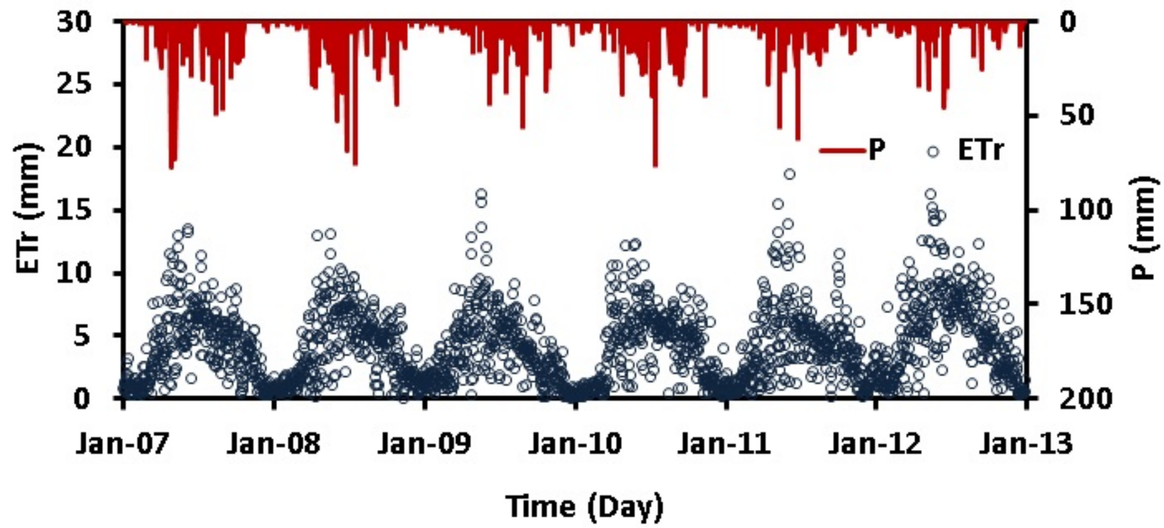

Figure 3. Daily precipitation (P) and reference evapotranspiration (ET_r) during the calibration (2008–2010) and validation (2011–2012) periods at the Mead Rainfed (US-Ne3) Site.

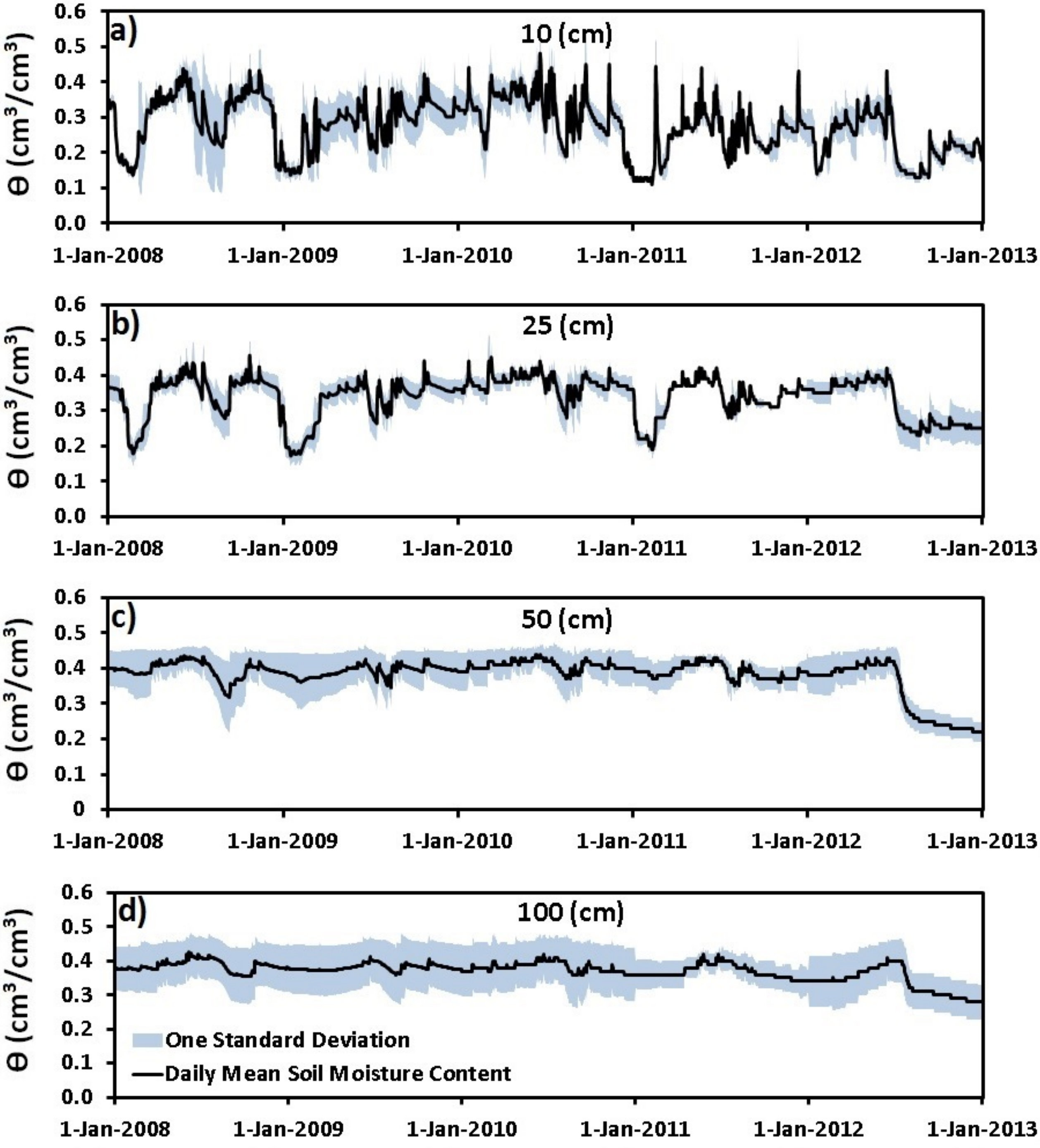

Figure 4. Temporal evolution of daily *SWC* (*θ)* at different soil depths. The black lines represent daily mean *SWC* (*θ)* calculated from TPs in 4 different locations at study site and the blue areas indicate one standard deviation.

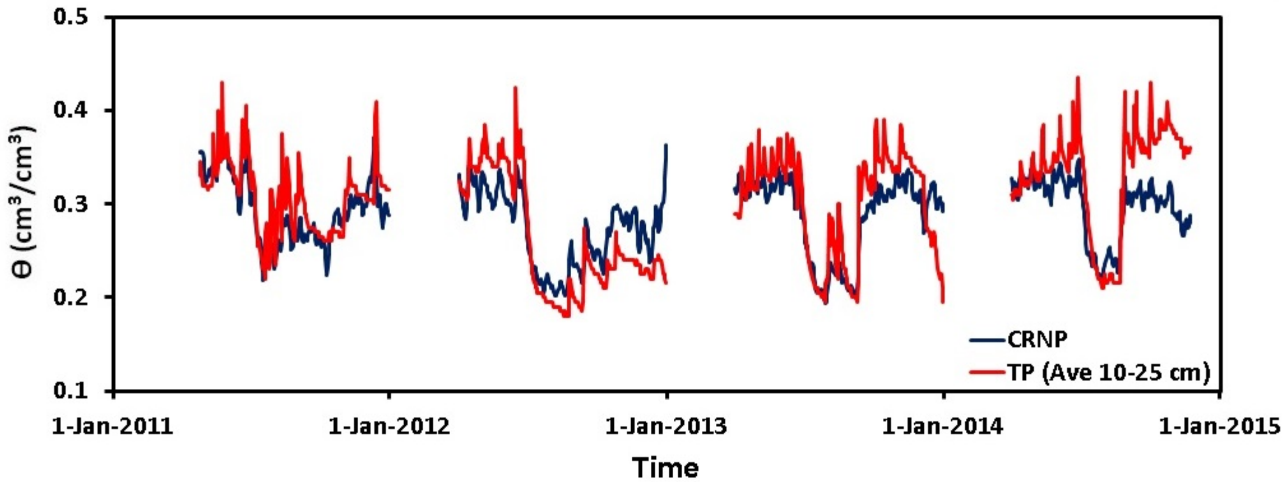

Figure 5. Time series of daily CRNP and spatial average TP *SWC* (*θ)* data.

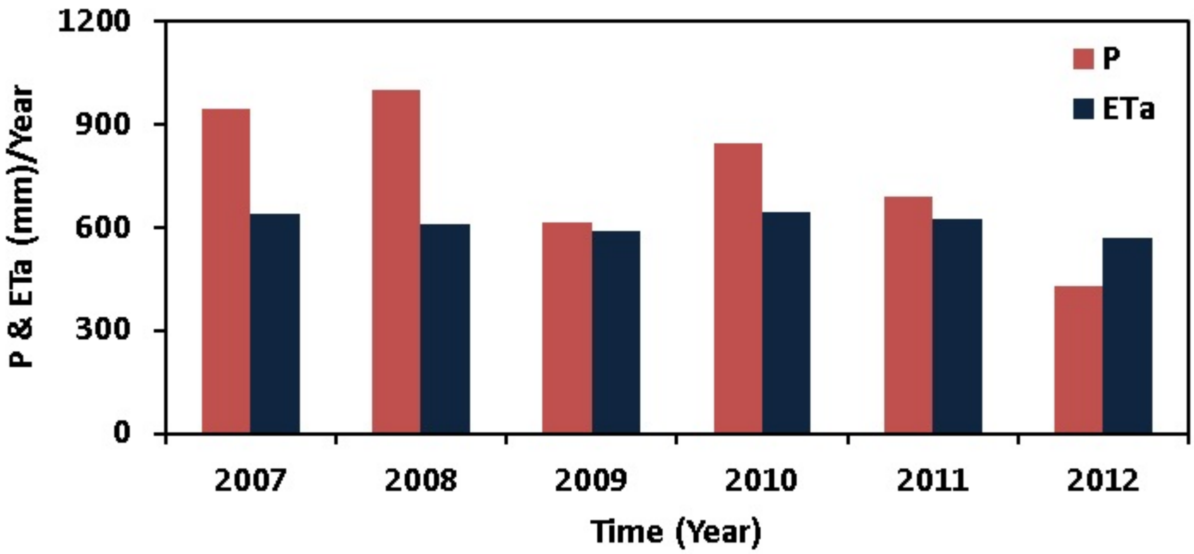

Figure 6. Annual precipitation (P) and annual actual evapotranspiration (ET_a) at the Mead Rainfed (US-Ne3) Site.

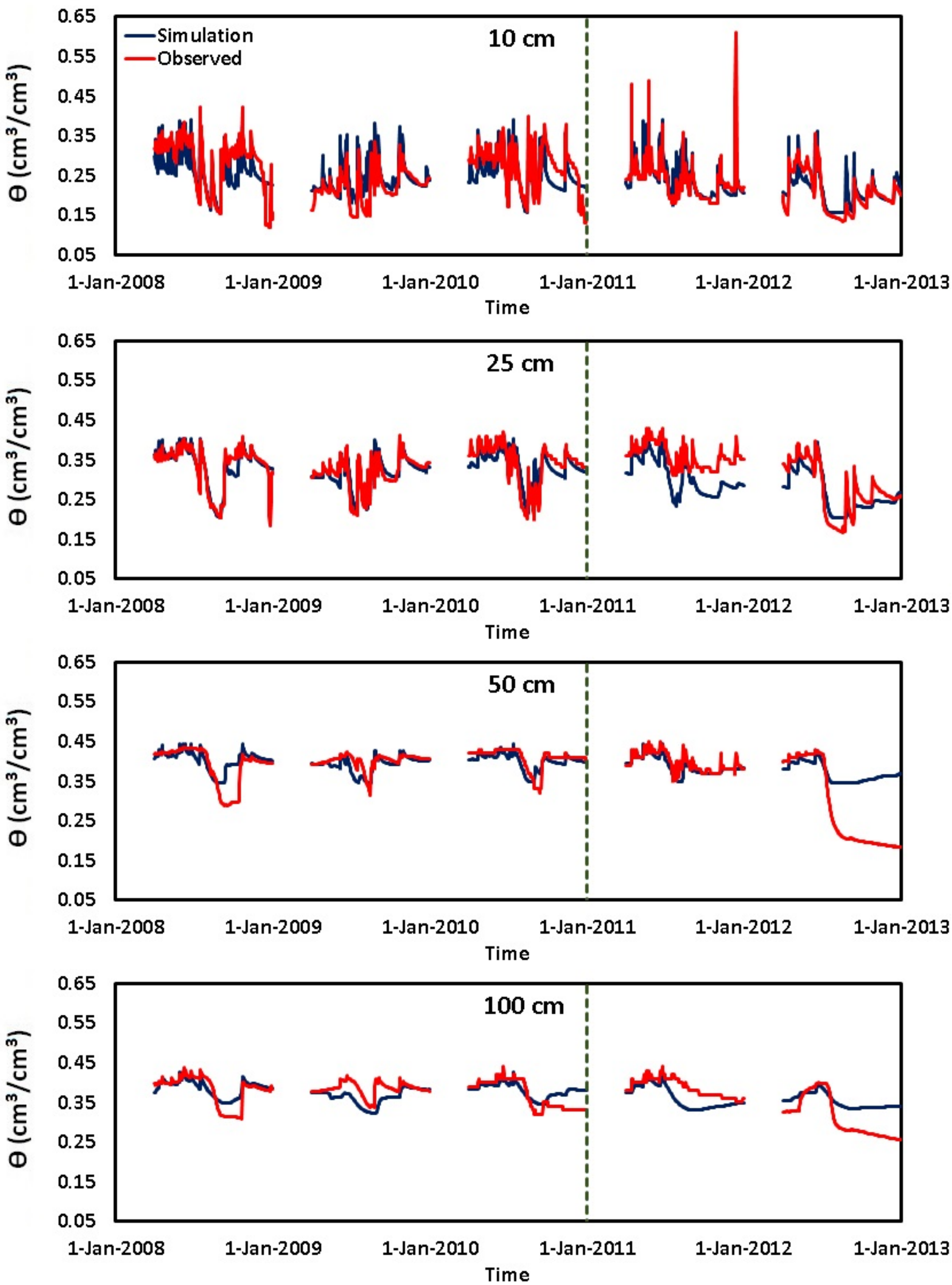

Figure 7. Daily observed and simulated *SWC* (*θ)* during the calibration (2008–2010) and validation (2011–2012) periods at TP 1 location. See supplemental figures for other comparisons.

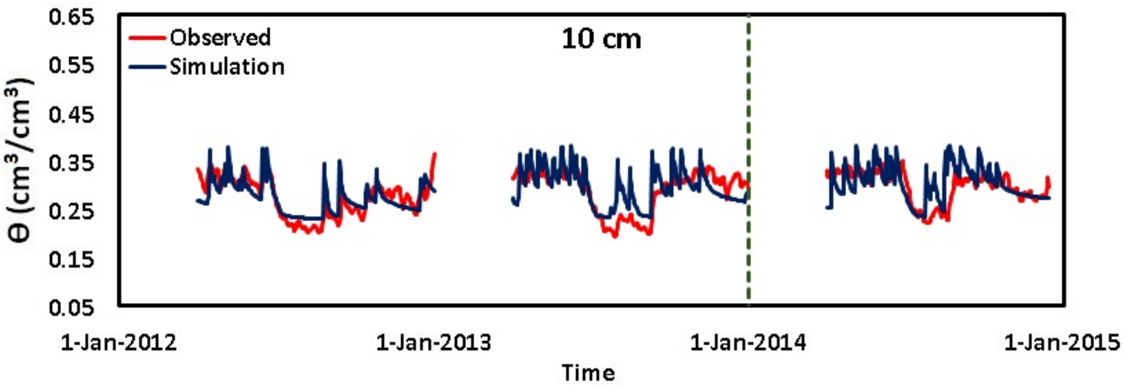

Figure 8. Daily observed and simulated *SWC* (*θ)* during the calibration (2012–2013) and validation (2014) periods at the location of Cosmic-Ray Neutron probe.

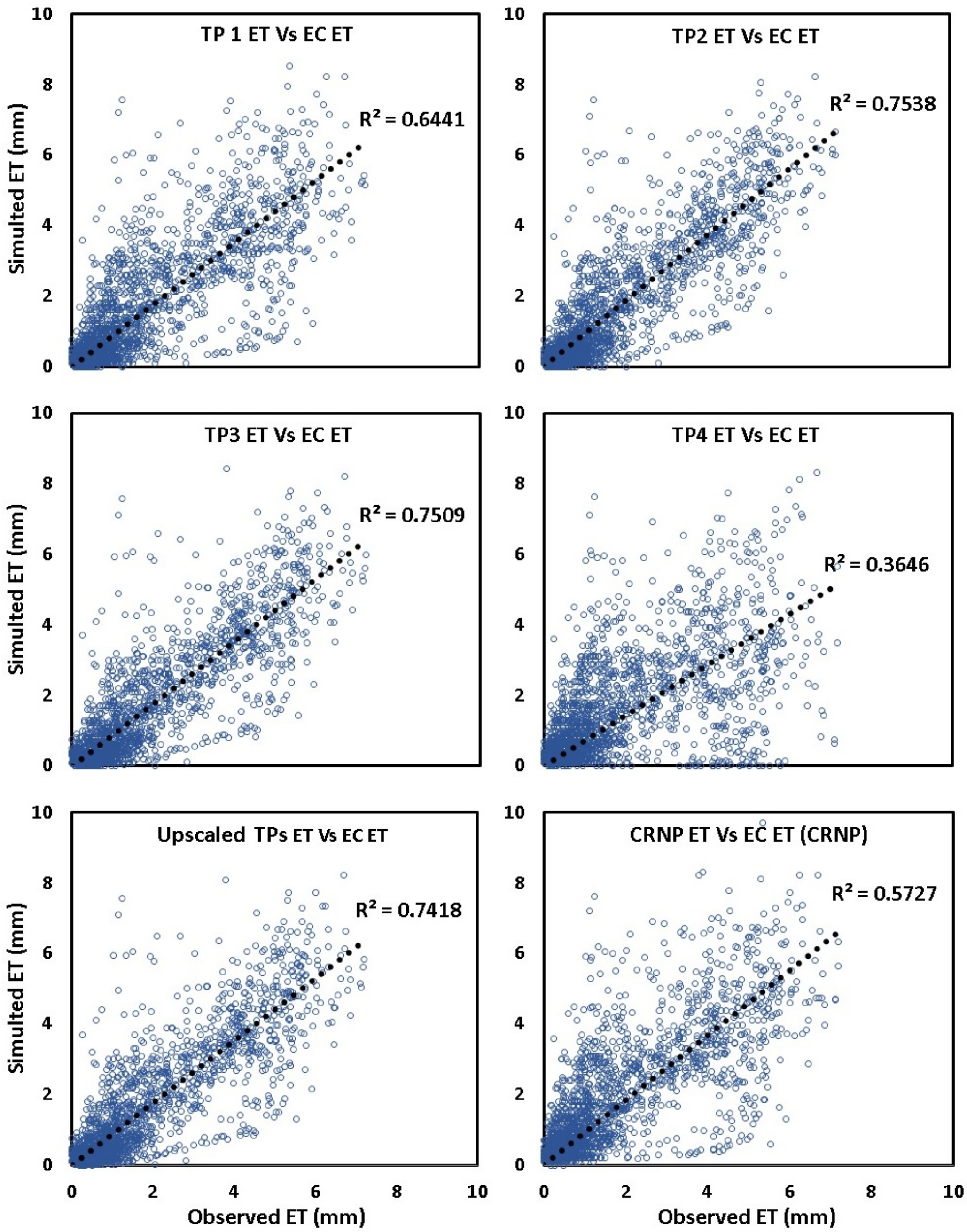

Figure 9. Simulated daily ET_a versus observed daily ET_a at different locations in the study site (2007-2012).

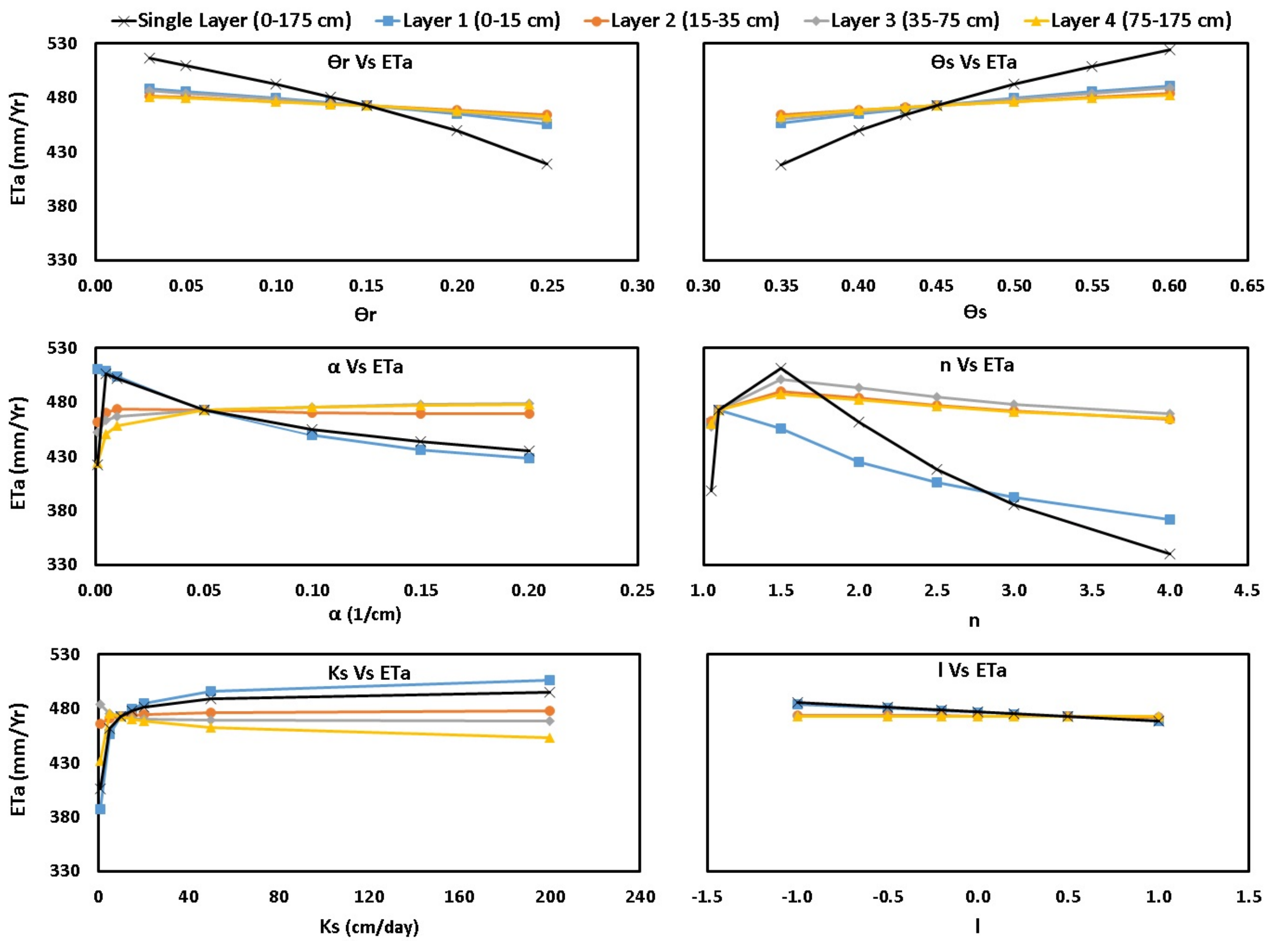

Figure 10. Sensitivity analysis of the effect of soil hydraulic parameters on average annual ET_a values (2007-2012) for a single homogeneous soil layer (6 parameters) and for a 4-layer soil profile (24 parameters).

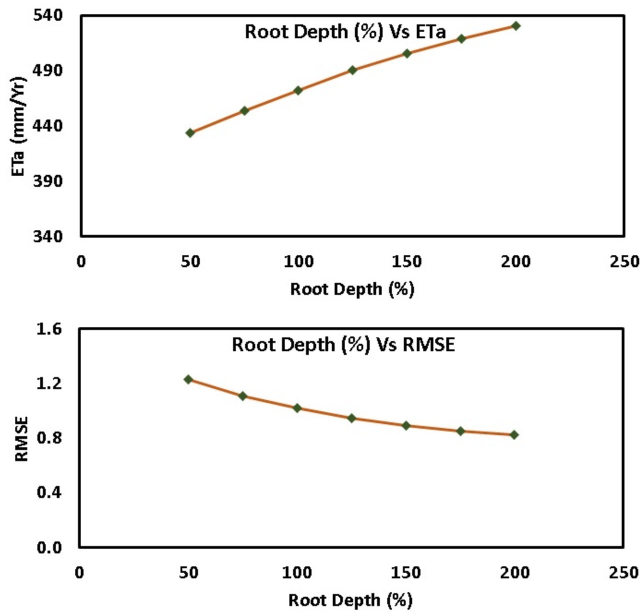

Figure 11. Sensitivity analysis of root depth on *ETa* estimation for a single homogeneous soil layer profile. Note that root depth is in terms of percent depth as it is dynamic over the growing period.

List of Tables

Table 1. Variability of soil texture in the study field based on Web Soil Survey data (http://websoilsurvey.sc.egov.usda.gov/App/HomePage.htm).

Table 2. Bounds of the van Genuchten parameters used for inverse modeling.

Table 3. Goodness-of-fit measures for simulated and observed *SWC* data at different depths during the calibration period (2008 to 2010) and validation period (2011-2012) at TPs locations.

Table 4. Goodness-of-fit measures for simulated and observed *SWC* data during the calibration period (2012 to 2013) and validation period (2014) at CRNP location.

Table 5. Optimized van Genuchten parameters in different locations at the study site. Note, 95% confidence intervals are in parentheses.

Table 6. Goodness-of-fit measures for simulated and observed daily ET_a during the simulation period (2007-2012) at study site.

Table 7. Summary of simulated yearly and average actual evapotranspiration (ET_a) (mm) and observed yearly and average actual evapotranspiration (ET_a) (mm) from Eddy-Covariance tower during 2007 to 2012.

Table 1. Variability of soil texture in the study field based on Web Soil Survey data (http://websoilsurvey.sc.egov.usda.gov/App/HomePage.htm).

Map Unit Symbol	Map Unit Name	Clay (%)	Silt (%)	Sand (%)	Hectares in Field	Percent of Field
3948	Fillmore silt loam, terrace, occasionally ponded	41.7	51.0	7.3	3.24	4.9%
7105	Yutan silty clay loam, terrace, 2 to 6 percent slopes, eroded	25.8	59.4	14.8	6.88	10.3%
7280	Tomek silt loam, 0 to 2 percent slopes	32.3	61.6	6.1	47.23	70.8%
7340	Filbert silt loam, 0 to 1 percent slopes	41.4	51.7	6.9	9.34	14.0%
Total Area of Field					66.69	100.0%

Table 2. Bounds of the van Genuchten parameters used for inverse modeling.

Soil Parameter	θ_r (-)	θ_s (-)	α (1/cm)	n (-)	K_s (cm/day)	l (-)
Range	0.03–0.30	0.3–0.6	0.001–0.200	1.01–6.00	1–200	-1–1

Table 3. Goodness-of-fit measures for simulated and observed *SWC* data at different depths during the calibration period (2008 to 2010) and validation period (2011-2012) at TPs locations. Note we assume a good fit as an RMSE between 0-0.03 cm^3/cm^3 and fair as between 0.03-0.06 cm^3/cm^3.

Location	Depth (cm)	Calibration Period (2008-2010)				Validation Period (2011-2012)			
		R^2	MAE (cm^3/cm^3)	RMSE (cm^3/cm^3)	NSE	R^2	MAE (cm^3/cm^3)	RMSE (cm^3/cm^3)	NSE
TP 1	10	0.542	0.024	0.036	0.533	0.532	0.016	0.033	0.503
	25	0.742	0.014	0.022	0.739	0.716	0.029	0.040	0.486
	50	0.409	0.013	0.023	0.407	0.603	0.041	0.074	0.157
	100	0.352	0.015	0.022	0.343	0.419	0.027	0.038	0.358
TP 2	10	0.330	0.044	0.066	0.305	0.287	0.047	0.061	0.052
	25	0.623	0.010	0.020	0.604	0.718	0.038	0.055	0.135
	50	0.551	0.015	0.026	0.074	0.683	0.040	0.055	0.202
	100	0.424	0.019	0.027	-2.055	0.344	0.048	0.073	-0.473
TP 3	10	0.269	0.034	0.051	0.256	0.534	0.086	0.102	-4.265
	25	0.512	0.011	0.017	0.509	0.852	0.010	0.015	0.793
	50	0.549	0.015	0.023	-0.214	0.658	0.022	0.033	0.652
	100	0.238	0.018	0.029	-3.156	0.669	0.018	0.025	0.178
TP 4	10	0.412	0.029	0.044	0.406	0.580	0.051	0.071	-0.116
	25	0.434	0.016	0.025	0.350	0.594	0.029	0.042	0.490
	50	0.151	0.009	0.015	-13.400	0.443	0.041	0.073	0.036
	100	0.001	0.013	0.021	-12.058	0.292	0.026	0.039	0.238

Table 4. Goodness-of-fit measures for simulated and observed *SWC* data during the calibration period (2012 to 2013) and validation period (2014) at CRNP location.

Location	Depth (cm)	Calibration Period (2012-2013)				Validation Period (2014)			
		R^2	MAE (cm^3/cm^3)	RMSE (cm^3/cm^3)	NSE	R^2	MAE (cm^3/cm^3)	RMSE (cm^3/cm^3)	NSE
CRNP	10	0.497	0.018	0.027	0.456	0.192	0.020	0.032	-0.310

Table 5. Optimized van Genuchten parameters in different locations at the study site. Note, 95% confidence intervals are in parentheses.

Location	Depth (cm)	θ_r (-)	θ_s (-)	α (1/cm)	n (-)	K_s(cm/day)	l (-)
TP 1	0-15	0.134 (0.130-0.137)	0.423 (0.417-0.429)	0.027 (0.026-0.027)	1.475 (1.456-1.494)	8.119 (7.965-8.273)	0.546 (0.525-0.567)
	15-35	0.136 (0.132-0.141)	0.408 (0.404-0.412)	0.007 (0.007-0.007)	1.345 (1.322-1.367)	11.540 (11.137-11.939)	0.480 (0.466-0.494)
	35-75	0.191 (0.188-0.194)	0.448 (0.443-0.453)	0.024 (0.024-0.025)	1.097 (1.088-1.105)	8.057 (7.879-8.235)	0.285 (0.278-0.292)
	75-175	0.071 (0.068-0.073)	0.430 (0.424-0.436)	0.025 (0.024-0.025)	1.069 (1.061-1.077)	9.807 (9.540-10.073)	0.364 (0.354-0.375)
TP 2	0-15	0.211 (0.195-0.227)	0.446 (0.431-0.461)	0.027 (0.018-0.035)	1.567 (1.431-1.703)	8.120 (4.660-11.580)	1.000 (0.411-1.589)
	15-35	0.197 (0.105-0.289)	0.434 (0.425-0.442)	0.006 (0.003-0.008)	1.191 (1.076-1.306)	8.655 (0.953-16.357)	0.022 (-0.194-0.238)
	35-75	0.110 (0-0.258)	0.424 (0.406-0.441)	0.015 (0.007-0.023)	1.239 (1.040-1.438)	4.605 (0-9.214)	0.723 (-1.210-2.655)
	75-175	0.109 (0-0.275)	0.408 (0.357-0.459)	0.020 (0-0.044)	1.302 (0.965-1.639)	6.780 (0-20.523)	0.000 (-0.045-0.045)
TP 3	0-15	0.281 (0.276-0.287)	0.464 (0.463-0.465)	0.035 (0.033-0.036)	1.487 (1.446-1.528)	7.096 (6.742-7.450)	0.400 (0.385-0.416)
	15-35	0.072 (0.069-0.075)	0.402 (0.398-0.407)	0.012 (0.011-0.012)	1.085 (1.076-1.095)	29.960 (28.470-31.457)	0.353 (0.340-0.367)
	35-75	0.081 (0.076-0.087)	0.498 (0.481-0.515)	0.037 (0.034-0.039)	1.128 (1.108-1.149)	24.440 (22.013-26.872)	0.527 (0.472-0.583)
	75-175	0.085 (0.077-0.092)	0.500 (0.482-0.518)	0.039 (0.036-0.042)	1.147 (1.124-1.170)	17.540 (15.995-19.088)	0.496 (0.454-0.539)
TP 4	0-15	0.082 (0.069-0.096)	0.481 (0.474-0.489)	0.034 (0.030-0.038)	1.172 (1.158-1.186)	7.773 (6.913-8.632)	0.953 (0.772-1.133)
	15-35	0.200 (0.175-0.225)	0.426 (0.420-0.433)	0.013 (0.010-0.017)	1.217 (1.173-1.262)	14.060 (9.248-18.873)	0.044 (0.027-0.061)
	35-75	0.250 (0.240-0.260)	0.477 (0.472-0.481)	0.009 (0.007-0.011)	1.079 (1.066-1.092)	1.045 (0.952-1.138)	0.353 (0.168-0.538)
	75-175	0.200 (0.185-0.214)	0.487 (0.481-0.494)	0.012 (0.009-0.014)	1.070 (1.057-1.083)	1.454 (1.146-1.762)	0.985 (0.706-1.264)
CRNP	0-15	0.100 (0.098-0.103)	0.392 (0.386-0.398)	0.019 (0.018-0.019)	1.054 (1.145-1.164)	6.931 (6.786-7.076)	0.547 (0.545-0.549)

Table 6. Goodness-of-fit measures for simulated and observed daily ET_a during the simulation period (2007-2012) at study site.

Location	R^2	MAE (mm/day)	RMSE (mm/day)	NSE
ET_p	0.510	1.359	1.992	0.340
TP 1	0.644	0.696	1.062	0.618
TP 2	0.754	0.610	0.907	0.746
TP 3	0.751	0.601	0.904	0.728
TP 4	0.365	0.878	1.387	0.168
TPs Weighted Average	0.742	0.599	0.911	0.714
CRNP	0.573	0.742	1.143	0.562

Table 7. Summary of simulated yearly and average actual evapotranspiration (ET_a) (mm) and observed yearly and average actual evapotranspiration (ET_a) (mm) from Eddy-Covariance tower during 2007 to 2012.

Location	Year						
	2007	2008	2009	2010	2011	2012	Average
ET_p	1048.5	987.9	989.4	1011.5	1025.7	1326.7	1064.9
EC	656.8	608.4	589.7	646.1	622.2	570.1	612.5
TP 1	646.1	629.0	559.8	642.1	573.9	415.5	579.5
TP 2	614.3	598.4	576.7	620.5	576.9	429.5	574.7
TP 3	529.0	556.1	556.4	590.4	549.8	405.2	545.4
TP 4	652.2	576.1	529.9	677.3	458.2	381.2	525.3
Upscaled TPs	613.9	564.1	556.3	600.3	547.7	405.9	548.0
CRNP	745.3	707.1	603.0	721.8	642.2	439.3	643.1